Nucleation of Ordered Ni Island Arrays on Au(111) by Surface-Lattice Dislocations

D. D. Chambliss, R. J. Wilson, and S. Chiang
IBM Research Division, Almaden Research Center, 650 Harry Road, San Jose, California 95120-6099
(Received 5 April 1990; revised manuscript received 28 November 1990)

Scanning tunneling microscopy of Ni deposited on Au(111) at room temperature reveals strikingly ordered island nucleation. Ni islands grow with spacing 73 Å along [1$\bar{2}$1] in rows 140 Å apart at surface-lattice dislocations induced by the Au(111) "herringbone" reconstruction. The island arrays are explained by a model in which Ni atoms diffuse on the surface and aggregate at these dislocations. Island size varies by more than the shot-noise limit, suggesting that the initial sticking probability is low when a diffusing atom encounters a dislocation.

PACS numbers: 68.35.Bs, 61.16.Di

The structure of metal films a few monolayers thick is strongly influenced by the way in which growth is nucleated. The need to understand nucleation and its relationship to properties such as strain and roughness is increasing as explanations are sought for surprising magnetic and magnetoresistive properties of ultrathin metal films and superlattices.[1,2] Recent experimental work has endeavored not only to minimize roughness and intermixing at metal-metal interfaces but also to exploit details of nucleation to create one-dimensional lateral structure on a nanometer scale.[3] We report here observations of ordered two-dimensional arrays of small metal islands. Examination of submonolayer Ni deposits on Au(111) at room temperature (RT) with the scanning tunneling microscope (STM) surprisingly reveals regular arrays of Ni islands. The islands form 73 Å apart along rows spaced by 140 Å; the arrays are coherent in (1000 Å)^2 domains. This new regular nucleation is caused by the long-range "herringbone" reconstruction of Au(111),[4] which induces periodic surface-lattice dislocations. The statistics of island size and number suggest that individual atoms diffusing on the surface can bind at these dislocations with a low sticking probability and act as nuclei for further aggregation.

The ultrahigh-vacuum STM apparatus has been described elsewhere.[5] The Au(111) crystal was cleaned by Ar-ion bombardment (1 keV) and annealed at 600° C for ≥ 5 min. After the sample was allowed to cool for at least 60 min to reach RT, it was exposed to Ni flux. This Ni, of 99.99% purity, was evaporated from an alumina-coated W basket at a rate of 0.04–0.4 monolayer (ML)/min. The pressure rise was $<2\times10^{-10}$ Torr, and no contamination of the surface with O or C was found by Auger electron spectroscopy (AES). The STM images shown here were obtained with tunnel currents of 0.5–2.0 nA. Each image was recorded in ~ 3 min, at least 1 h after deposition.

The wide-area scan in Fig. 1 shows that 0.1 ML of Ni deposited on Au(111) at RT forms ordered rows of islands with nearly uniform spacing. The average center-to-center spacing is 73 Å between islands in a row along [1$\bar{2}$1] and 140 Å between rows. Every wide terrace (>500 Å) we have seen is covered with such an array. The island arrays occur in three equivalent orientations related by 12° rotations. Differently oriented domains may occur on the same terrace, and the domain size is comparable to the typical terrace width of 2000 Å. Within a domain, some deviations from perfect ordering are seen, but the island positions remain coherent over the full domain size. In narrower-scan images, the islands all appear to have a similar size of ~ 140 atoms. In samples prepared with different Ni exposures, the island spacing remains the same while the average island size varies in proportion to Ni coverage. At coverages $\gtrsim 0.6$ ML the islands start to connect into monolayer ribbons in the [1$\bar{2}$1] directions, with some second-layer growth evident.[6] The apparent island height (1.90 ± 0.05 Å), measured for a range of bias voltages, is consistent with a single atomic layer of Ni pseudomorphic

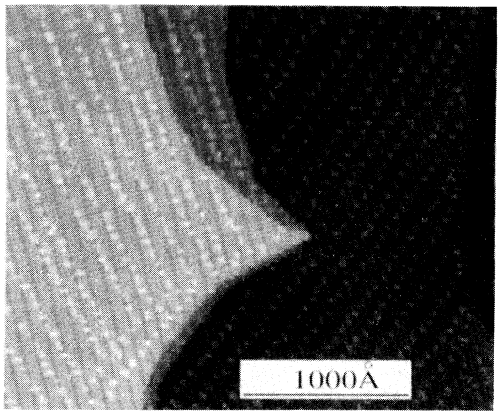

FIG. 1. STM image of 0.11 ML Ni on Au(111). Several atomically flat Au terraces are seen, separated by steps of single-atom height. Small light dots on each terrace are monolayer Ni islands, in rows along [1$\bar{2}$1]. Deposition rate is 0.4 ML/min. Island shapes are not resolved here because their size is comparable to the pixel size (10 Å)^2. Sample bias is $V_s = 2.0$ V.

with Au(111), and is sufficiently different from the Au(111) step height (2.35 Å) that Au steps and Ni deposits are readily distinguished.

Images of smaller areas show clearly that Ni islands are found at particular sites in the Au(111) herringbone,[4] in which the reconstruction alternates between two equivalent directions of uniaxial contraction in 140-Å-wide domains. In each domain, the registry of surface Au atoms varies between hollow sites of face-centered-cubic (fcc) and hexagonal-close-packed (hcp) stacking, to fit 23 atomic rows in 22 lattice spacings.[7] The fcc regions are wider than the hcp regions. The fcc-hcp transitions appear as ridges to the STM [Fig. 2(a)] because surface atoms near bridge sites rest ~0.2 Å higher than in hollow sites. When the clean surface is exposed to Ni atoms, islands form predominantly at the "elbows" where the ridges change direction by 120° [Fig. 2(b)]. The elbows, and thus the Ni islands, lie on the boundaries between the uniaxial domains. The direction of the elbows, and their appearance, alternates from one domain boundary to the next [Fig. 2(a)]. On one boundary, the hcp regions are very narrow, apparently "pinched off" by the ridges. On the next boundary, the hcp and fcc regions are nearly equal; these elbows might be described as "bulged." On both elbow types, the small islands formed at low Ni coverages are found at the apexes of the bends in ridges denoted "type x," which are distinguished from "type-y" ridges by their characteristic shapes at the elbows [Figs. 2(c) and 2(d)]. The preference for certain island sites suggests a local distortion of electronic or atomic structure that tends to capture Ni atoms that are diffusing on the surface. An atom attached to such a site would then be a nucleus for aggregation of a larger island.

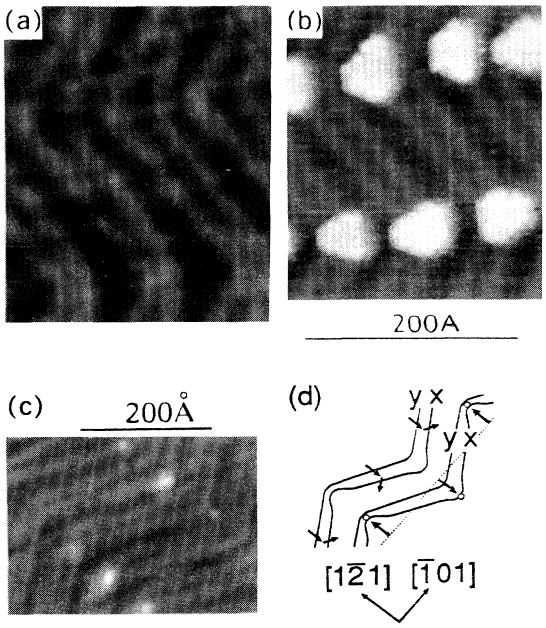

FIG. 2. Correlation of Ni island nucleation with Au reconstruction. (a) Typical reconstructed section of large terrace on clean Au(111). Light zigzagging bands are ~0.2-Å-high ridges where atoms are near bridge sites. "Elbows" in ridges lie on two nearly horizontal domain boundaries. The lower boundary contains "pinched" elbows; the upper one, "bulged" elbows. $V_s = -2.0$ V. (b) Completed nucleation and polygonal shape of Ni islands at 0.14 ML. $V_s = -0.61$ V, deposition rate 0.1 ML/min. Of thousands of islands observed in dozens of STM images that reveal both islands and reconstruction ridges, ~99% form at these elbow sites. In (b) and (c) a nonlinear gray scale is used to make ridges visible. (c) Nucleation of Ni islands at elbows at $\theta = 0.01$. Three islands are seen on each of two domain boundaries of the herringbone pattern, running diagonally from upper left to lower right. $V_s = -1.11$ V, deposition rate 0.05 ML/min. (d) Sketch of herringbone pattern and nucleation sites. Two pairs of ridges are shown as dark bands. Arrows on the upper pair show directions of Burgers vectors, which alternate in type-x ridge and remain constant in type-y ridge. On the lower pair, small circles mark island sites [cf. (c)], located symmetrically about the central axis of the type-x ridge (fine line).

The crystallography of the reconstruction explains why the elbows have distorted structures: Each elbow contains a dislocation of the surface lattice. In the uniaxial domains, the ridges are partial surface dislocations whose structure is known,[7,8] and examination of their Burgers vectors [Fig. 2(d)] explains the island nucleation at type-x elbows. A type-x ridge is a series of dislocation segments with different Burgers vectors. The surface atoms in these segments occupy bridge sites of two different orientations corresponding to these Burgers vectors. Where the segments meet, a dislocation of the two-dimensional lattice is found, whose Burgers vector is the difference between those of the two segments. A type-y ridge, in contrast, is a continuous partial surface dislocation, with a single Burgers vector. The surface atoms there lie in bridge sites of the same orientation, and the deviations from bulk bond topology occur only between the first and second layers. Thus within the first layer the bond geometry is that of a (strained) hexagonal layer everywhere except at the apexes of type-x ridges, where deviations must occur to accommodate an extra atomic row. Near steps and at boundaries between two different herringbone orientations, the herringbone reconstruction is disturbed. In these areas, the various ways ridges connect also involve surface-lattice dislocations that nucleate Ni islands.

While it is simplest to illustrate the surface-lattice dislocations as localized at a single atomic site,[6] the width of the Au(111) dislocation ridges leads us to expect considerable relaxation of the surface lattice near the dislocation. Atomic-resolution images of Au(111) (Fig. 3) show that the distortions extend for several lattice constants. Figure 3(a) shows a region around a "pinched" elbow. In this area, the image reveals sites

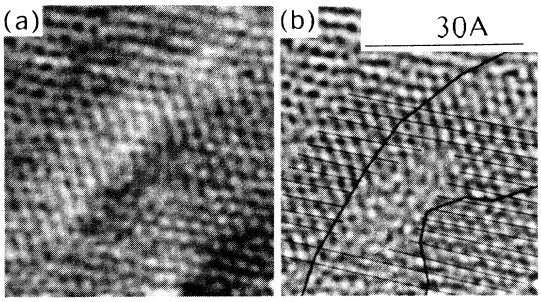

FIG. 3. Atomic structure of Au(111) surface-lattice dislocation. (a) STM image of "pinched" elbow, taken under near-contact conditions ($V_s = -1.3$ mV $I = 1.0$ nA). Elbow orientation is that of those in lower left of Fig. 2(d). (b) Bandpass-filtered image of (a). Heavy lines mark partial-dislocation ridges. Fine lines mark atomic rows in ordered regions; surface-lattice dislocation is revealed by number of lines on either side (13 vs 14).

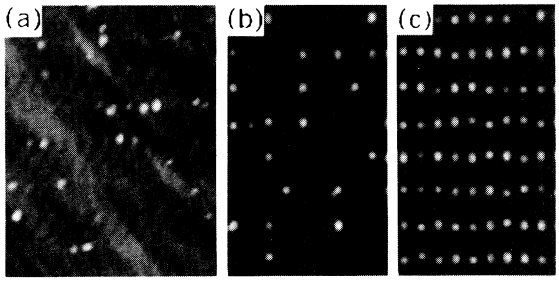

FIG. 4. (a) STM image of Au(111)+0.01 ML Ni. $V_s = -1.5$ V, deposition rate 0.05 ML/min. Many elbow sites do not have islands. (b) Island distribution in simulation with $s_0 = 0.005$ at $\theta = 0.01$. Atoms are too small to show individually, so pixel intensities vary with island size. This simulates rapid-scan STM imaging with a blunt tip [as in (a)]. (c) Island distribution in simulation with $s_0 = 1$ at $\theta = 0.01$. Different gray scales are used in (b) and (c) to optimize visibility.

that deviate from sixfold-bond geometry. But some unusual blurred features are not readily interpreted as individual atoms. It is possible that tip-sample interactions, which complicate the interpretation of atomic-resolution data,[9,10] might cause atomic rearrangements at these extended defects. Indeed, variability in the elbow shapes is seen in lower-resolution images, suggesting that a variety of atomic configurations have nearly the same energy. Nevertheless, the structure of the well-ordered lattice surrounding a dislocation, as in Fig. 3(b), consistently shows that one fewer atomic row enters at one side (here, the upper left) than emerges at the other, which confirms the presence of a dislocation. Features that do not require lateral atomic resolution, such as island positions and heights and the lateral position of Au(111) reconstruction ridges, are imaged much more reliably.

This highly ordered island formation suggests unprecedented possibilities for the fabrication of equivalent structures with a well-defined spacing on a nanometer scale. An important issue is the uniformity of island size. The simplest model for island formation is that Ni atoms diffuse on the surface and aggregate with equal probability at each elbow. In such a Poisson process the fraction of islands with size N is $p_N(x) = x^N e^{-x}/N!$, where $x = \langle N \rangle$ is the average number of atoms per elbow at coverage θ ML; the lattice constant and elbow spacing imply $x \simeq 1400\theta$. The rms island-size variation would be $\sigma_N \equiv \langle N^2 - \langle N \rangle^2 \rangle^{1/2} = \langle N \rangle^{1/2}$ (shot noise). The observed variation is actually much greater, particularly at low coverage (Table I, Fig. 4). This is not surprising, since capture probabilities should vary with the number of atoms already at a site, both because larger islands have a larger perimeter and, more important in this case, the sticking coefficient s_i at an island-perimeter site should be different from that at an elbow site with no Ni atoms, s_0. If $s_i \gg s_0$, there will be greater heterogeneity since atoms tend to be captured by existing islands rather than to nucleate islands at new sites. Heterogeneity would also be greater if clusters as well as single atoms were mobile on the surface. Mobile clusters do not dominate the island nucleation here, since island uniformity does not depend strongly on deposition rate. Furthermore, several STM images show apparently single-atom islands at elbows. But a few islands ($\sim 1\%$) that are observed away from any surface-lattice dislocations may have originated as clusters that grew large enough to be immobile before reaching an elbow. Another cause of island heterogeneity is the variability in elbow structure and spacing, associated mainly with the presence of atomic steps.

TABLE I. Statistics of Ni island nucleation on Au(111).

Model	Fraction of sites vacant at $\theta = 0.01$	Island size variation σ_N at $\langle N \rangle = 200$	nn pair correlation γ at $\theta = 0.01$
Poisson	$< 10^{-6}$	14.1	1
Simulation, $s_0 = 1$	< 0.002	20 ± 1	...
Simulation, $s_0 = 0.005$	0.61 ± 0.04	100 ± 10	0.84 ± 0.08
Experiment	0.70 ± 0.02	65 ± 20	1.14 ± 0.18

We have used Monte Carlo simulations to examine the importance of s_0.[11] In these, atoms land one at a time and walk at random on a hexagonal lattice of 992×992 sites [~ 2500 Å wide for Au(111)] with periodic boundary conditions. Of the sites, 512 are marked as identical nucleation centers spaced like Au(111) elbows. Each time an atom reaches a marked site it has probability s_0 of stopping. Once an island is nucleated we assume its perimeter sites have unity sticking ($s_i = 1$) because of the extra bond coordination there. Islands are assumed to

have nearly regular hexagonal shapes like those observed experimentally [Fig. 2(b)]. Computation is accelerated by dividing the lattice into overlapping cells each containing one island or marked site at its center, and replacing the random walk within a cell with a single step to the center or to one of the cell boundary sites, with probabilities determined by the island size and the starting position in the cell.[11] These steps are repeated until the atom adheres to an island. Reasonable agreement with experiment occurs for $0.03 > s_0 > 0.003$ (Table I, Fig. 4). The results for $s_0 = 1$ are quite close to Poisson statistics. Thus island uniformity much closer to the shot-noise limit should be attainable if s_0 could be increased to near unity, perhaps by using a lower substrate temperature.

The spatial distribution of islands at low θ [Fig. 4(a)] appears random, like independently nucleated islands rather than mobile clusters whose spacing is fixed by attractive or repulsive interactions. This is quantified in the nearest-neighbor-site pair correlation $\gamma = \langle \rho(\alpha)\rho(\alpha \pm 1)\rangle_{nn} / \langle \rho(\alpha)\rangle^2$, where $\rho(\alpha) = 1$ if the elbow site α has an island and 0 if not, and $\langle\rangle_{nn}$ averages over pairs $(\alpha, \alpha \pm 1)$ of neighboring sites on the same domain wall. At low coverage, an interaction between Ni clusters, perhaps mediated by distortions of the substrate, should cause $\gamma < 1$ ($\gamma > 1$) for a repulsion (attraction). The experimental value of γ is close to 1 (Table I). The simulations predict $\gamma < 1$ since nucleated islands capture atoms and suppress island nucleation nearby. The value of γ could, however, be affected by steps and elbow variability, which the simulations did not include.

The regularity of this nucleation mechanism invites speculation about its possible applications. Ni/Au(111) may be an appealing system for studies of size effects on electronic and magnetic properties, since the island size and spacing are easily predicted. It could also be interesting for examining the chemical difference between steps and terraces. Island uniformity might be improved by lowering the substrate temperature, as noted above. The Au(111) elbow sites can presumably nucleate growth of other metals as well. The Au(111) reconstruction ridges are like misfit dislocations seen in metal heteroepitaxy systems, so similar surface-lattice dislocations could cause ordered nucleation phenomena in other substrate systems. Well-characterized monolayer island arrays might further be used as seed layers for growth by diffusion-limited or electric-field-limited processes to produce films with unusual structure on a nanometer scale.

In summary, we have shown that Ni islands grow with nearly uniform spacing on Au(111). We have identified the mechanism in the atomic structure of reconstructed Au(111), both by analyzing the regions where the reconstruction is well understood and by imaging directly the dislocation sites. Simulations have shown that the island statistics are consistent with a model of diffusing and aggregating Ni atoms, if a low initial sticking probability is assumed. It is well known that island growth can be induced by defects like emerging bulk dislocations or by homogeneous nucleation under rapid deposition. The surprise here is that the annealed Au(111) surface, after reconstructing to reduce its total energy, includes an array of intrinsic "defects" which control Ni layer growth. The dependence of island structure of a metal monolayer on the atomic structure of the previous layer is a concern in attempts to grow metal overlayers and superlattices. Knowledge of such dependence also offers new possibilities for lateral patterning of such films on a nanometer scale. A full understanding of near-monolayer metal films requires further analysis of the relationship of atomic structure to film nucleation.

This work was partially supported by the Office of Naval Research (N00014-89-C-0099). We are grateful to J. P. Toennies for the loan of the Au(111) crystal, and to Barbara Jones and Frank Herman for helpful discussions.

[1] S. S. P. Parkin, S. Fan, N. More, and K. P. Roche, Phys. Rev. Lett. **64**, 2304 (1990).

[2] M. N. Baibich, J. M. Broto, A. Fert, F. Nguyen Van Dau, F. Petroff, P. Etienne, G. Creuzet, A. Friederich, and J. Chazelas, Phys. Rev. Lett. **61**, 2472 (1988).

[3] P. M. Petroff, A. Y. Cho, F. K. Reinhart, A. C. Gossard, and W. Wiegmann, Phys. Rev. Lett. **48**, 170 (1982).

[4] D. D. Chambliss and R. J. Wilson, J. Vac. Sci. Technol. A (to be published).

[5] S. Chiang, R. J. Wilson, Ch. Gerber, and V. M. Hallmark, J. Vac. Sci. Technol. A **6**, 386 (1988).

[6] D. D. Chambliss, R. J. Wilson, and S. Chiang, J. Vac. Sci. Technol. A (to be published).

[7] Ch. Wöll, S. Chiang, R. J. Wilson, and P. H. Lippel, Phys. Rev. B **39**, 7988 (1989).

[8] U. Harten, A. M. Lahee, J. P. Toennies, and Ch. Wöll, Phys. Rev. Lett. **54**, 2619 (1985).

[9] P. H. Lippel, R. J. Wilson, M. D. Miller, Ch. Wöll, and S. Chiang, Phys. Rev. Lett. **62**, 171 (1989).

[10] J. Wintterlin, J. Wiechers, H. Brune, T. Gritsch, and J. Behm, Phys. Rev. Lett. **62**, 59 (1989).

[11] D. D. Chambliss, S. Chiang, and R. J. Wilson (to be published).

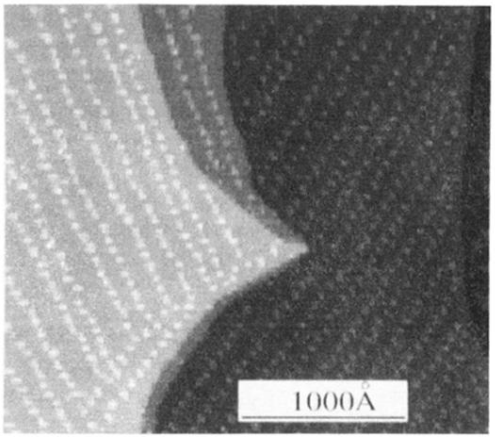

FIG. 1. STM image of 0.11 ML Ni on Au(111). Several atomically flat Au terraces are seen, separated by steps of single-atom height. Small light dots on each terrace are monolayer Ni islands, in rows along $[1\bar{2}1]$. Deposition rate is 0.4 ML/min. Island shapes are not resolved here because their size is comparable to the pixel size $(10\ \text{Å})^2$. Sample bias is $V_s = 2.0$ V.

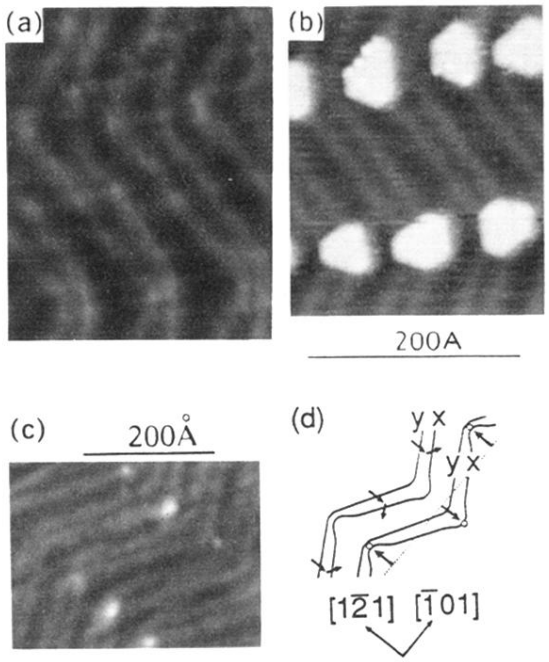

FIG. 2. Correlation of Ni island nucleation with Au reconstruction. (a) Typical reconstructed section of large terrace on clean Au(111). Light zigzagging bands are ~0.2-Å-high ridges where atoms are near bridge sites. "Elbows" in ridges lie on two nearly horizontal domain boundaries. The lower boundary contains "pinched" elbows; the upper one, "bulged" elbows. $V_s = -2.0$ V. (b) Completed nucleation and polygonal shape of Ni islands at 0.14 ML. $V_s = -0.61$ V, deposition rate 0.1 ML/min. Of thousands of islands observed in dozens of STM images that reveal both islands and reconstruction ridges, ~99% form at these elbow sites. In (b) and (c) a nonlinear gray scale is used to make ridges visible. (c) Nucleation of Ni islands at elbows at $\theta = 0.01$. Three islands are seen on each of two domain boundaries of the herringbone pattern, running diagonally from upper left to lower right. $V_s = -1.11$ V, deposition rate 0.05 ML/min. (d) Sketch of herringbone pattern and nucleation sites. Two pairs of ridges are shown as dark bands. Arrows on the upper pair show directions of Burgers vectors, which alternate in type-x ridge and remain constant in type-y ridge. On the lower pair, small circles mark island sites [cf. (c)], located symmetrically about the central axis of the type-x ridge (fine line).

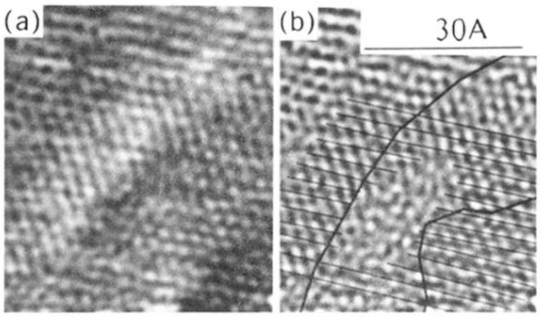

FIG. 3. Atomic structure of Au(111) surface-lattice dislocation. (a) STM image of "pinched" elbow, taken under near-contact conditions ($V_s = -1.3$ mV $I = 1.0$ nA). Elbow orientation is that of those in lower left of Fig. 2(d). (b) Bandpass-filtered image of (a). Heavy lines mark partial-dislocation ridges. Fine lines mark atomic rows in ordered regions; surface-lattice dislocation is revealed by number of lines on either side (13 vs 14).

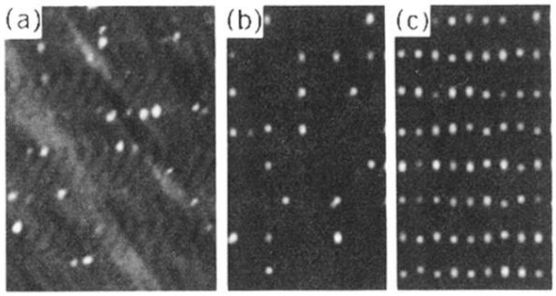

FIG. 4. (a) STM image of Au(111)+0.01 ML Ni. $V_s = -1.5$ V, deposition rate 0.05 ML/min. Many elbow sites do not have islands. (b) Island distribution in simulation with $s_0 = 0.005$ at $\theta = 0.01$. Atoms are too small to show individually, so pixel intensities vary with island size. This simulates rapid-scan STM imaging with a blunt tip [as in (a)]. (c) Island distribution in simulation with $s_0 = 1$ at $\theta = 0.01$. Different gray scales are used in (b) and (c) to optimize visibility.